



Article

Hygrothermal Behaviour of Continuous Air Chambers on Stone Panels Façades through CFD and IRT

Carlos Lerma ^{1,*}, Ángeles Mas ¹, Enrique Gil ² and Jose Vercher ¹

¹ Department Architectural Constructions, Universitat Politècnica de València, Camino de Vera s/n, 46022 Valencia, Spain

² Department of Continuous Medium Mechanics and Theory of Structures, Universitat Politècnica de València, Camino de Vera s/n, 46022 Valencia, Spain

* Correspondence: clerma@csa.upv.es

Received: 28 June 2019; Accepted: 24 July 2019; Published: 26 July 2019



Abstract: Façades of buildings with stone cladding are widely used in contemporary architecture. This research work analyses the aerodynamic, thermal and relative humidity behaviour of this type of façade. One of the main novelties of the article is the analysis of air flow and temperature of the air chamber through finite elements with computational fluid dynamics (CFD). Ten three-dimensional models were designed to study the various parameters that influence the behaviour of the façade, including the thickness of the air chamber and the velocity of the outside air. A qualitative and quantitative analysis of temperature and humidity makes it possible to determine the areas susceptible to generating condensation. Infrared thermography (IRT) is used to obtain the actual outside temperature, which is used in the validation of finite element models. The temperature is reduced by 47% with air chambers of 3 cm instead of 1 cm with soft outside air velocity, and by up to 60% with moderate air velocity. In these cases, relative humidity increases by 96% and 74%, respectively. When the results obtained in CFD vary considerably in a particular area with respect to IRT, a possible pathology is identified. This work provides better knowledge on the durability of material and façades.

Keywords: CFD; IRT; air chamber; stone panels; building materials; finite elements; natural convection

1. Introduction

In Europe, a large number of buildings are constructed with stone coverings. Stone panels are supported only by certain anchorage points, leaving a joint on each of the four edges of the stone. When the wall is designed according to the ‘rainscreen principle’ [1], air pressure inside the cavity will be the same as that outside the cavity. For all enclosures of buildings, thermal behaviour and possible condensation are studied in order to avoid problems related to humidity and deterioration of the materials. Any enclosure has important functions to perform, requiring stability, thermal insulation, and air- and watertightness, among other things. A good hygrothermal functioning of the enclosure depends on the construction materials, and above all on a good construction design. Today, enclosures of buildings with stone cladding are constructed comprising an interior sheet that serves as a support for thermal insulation, and an open air chamber, ventilated through the joints of the outer sheet. The outer layer is composed of stone cladding.

Different research works have addressed the study of temperature and natural convection in building façades for decades. Numerical solutions have been carried out for natural convection heat transfer in a square cavity [2], the natural convection problem in an enclosure with one thick vertical wall [3], and heat transfer with two vertical walls, one conducting and one insulated [4]. Conduction along with the natural convection of fluid flow in enclosures has also been studied [5].

Already in 1984, Kuehn and Maldonado [6] had performed one- and two-dimensional calculations under various temporal conditions. Theoretical calculations of thermal resistance, albeit in other types of enclosures, have also been studied [7]. However, thermal calculations have already been made with finite elements in specific parts of buildings, such as in the encounter between enclosures, slabs and cantilevers [8]. Only the effect of air and thermal radiation is considered, not, for example, rainwater, which has also been studied previously [9]. It is therefore a great novelty to use a finite element program for modelling using Computational Fluid Dynamics (CFD) and applying it to the enclosure of a building to study the hygrothermal behaviour of the ventilated air chamber.

Some of the advantages of cavity walls include [10]: the reduction of construction time, the possibility of using materials from the area to reduce transport costs, increased energy efficiency.

The thermal contribution of the air chamber is small, but it has an essential function in the control and drying of rainwater. In the air chamber, there is an upward movement of the air due to the difference in temperature that occurs between the outer and inner leaf [11]. The air cavity between both layers acts as a capillary break and a channel for drainage and drying [12].

Various parameters can influence the air conditions in the chamber, such as building exposure, exterior leaf, wind speed and direction, type of openings, or chamber dimensions [13–15], as well as environmental conditions [16,17]. Vertical air flows depend on density; however, if forced convection occurs, the flow can be multidirectional and highly turbulent [18].

Simulations were performed with the software Autodesk Simulation CFD 2019. This is finite element software for fluid flow analysis and thermal behaviour with steady or transient modes for 2D and 3D models. This program is very powerful, and is used in other fields of engineering for the design of aircraft, racing cars, and engines. All parameters and characteristics of the simulations were carried out in accordance with the Autodesk application manual [19].

Infrared thermography (IRT) is a powerful non-contact imaging technique, suitable for the protection of cultural heritage [20]. The appropriate conservation measures for a particular building can only be planned and carried out when an accurate damage diagnosis is made. In this sense, the application of IRT in the pathology study of façades with posterior ventilation with stone panels is interesting. In this way, consistent information about the materials is provided, as well as the factors, processes and state of deterioration [21].

Non-destructive techniques such as IRT facilitate the study and further the understanding of materials and construction processes, without needing to inflict damage on the building. Most buildings have been built with different types of stone. There are architectural, constructive or artistic considerations to choosing the material, such as the proximity of quarries and the ease of extraction from them.

Many other previous studies have already established a link between IRT and the detection of defects in stone materials of a building [22] or in a laboratory [23], although in these studies, the thermographic data for different points of the walls are interpreted by means of graphs [24]. Those areas where thermal discontinuities occur are usually where defects in the material are located. On the other hand, those points which display a similar temperature demonstrate thermal inertia, i.e., the tendency of an element to resist thermal changes, and this depends on the characteristics of the material, the moisture present, and any damage [25]. Thermography has also been used to detect moist areas [22] or using IRT to detect air leakage points [26].

The thermal pattern of a material largely depends on its characteristics (thermal diffusion, porosity, density, etc.). The possibility of being able to clearly visualise the defects of a material depends on the difference between the thermal characteristics of the material and the absence of homogeneity [27].

A methodology is developed for pathology detection in façades of stone panels with continuous air chambers, by comparing the results obtained with an infrared camera and CFD simulations. Substantial validation work was carried out, verifying that the same results were obtained through CFD than with IRT. Afterwards, CFD simulations and IRT of real cases were carried out. Where the results obtained in the simulation varied considerably in a specific area with respect to thermography,

a possible pathology was identified. This work focuses on buildings located in Valencia (Spain) to better understand the hygrothermal behaviour of the enclosures of stone panels.

2. Methods

2.1. Case Study

Several three-dimensional models were designed to carry out this research. A different model describes each of the cases explained below, which are those that we consider of greatest interest in analysing the hygrothermal response of the air chamber of an enclosure with stone cladding.

The prescriptions established by the current Spanish standard on Natural Stone products allow the development of these models. This standard is called Construction of Slabs for Façades with Natural Stone (UNE 22203: 2011) [28]. This standard establishes that the joints in cladding subjects with ventilated façade anchors must be 2 mm wide in general, and must be able to reach up to 6 mm for large cladding. Likewise, in order to improve the ventilation of the air chamber, vertical joints of 10 mm should be provided at distances of every 6 m, and horizontal joints of 15 mm should be provided at the level of each floor. The perimeter joints must be 10 mm, and the structural joints must be respected, being less than 2 cm. Regarding the air chamber, the standard states that it must have a minimum dimension of 3 cm. The maximum dimension of the air chamber is 10 cm, according to the Spanish standard CTE-DB-HS [29].

The phenomenon is, in reality, very complex; therefore, in the present study, some simplifications were carried out. Following the prescriptions of the standard, 5 models were elaborated according to the geometry. Each model consists of a band 50 cm wide and 3 stories high, simulating the conditions of a real building (Figure 1).

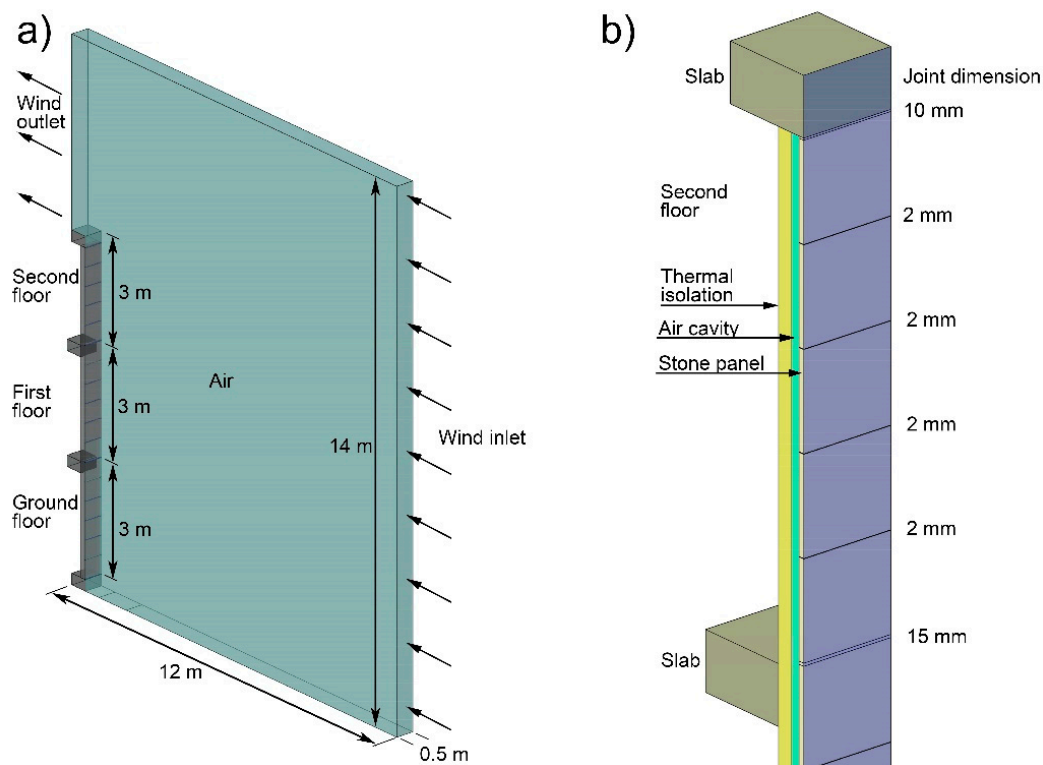


Figure 1. Geometry of the models used in the simulations: (a) General view and (b) detail view.

The overall volume is $12 \times 14 \times 0.5 \text{ m}^3$. The distance between the slabs of the building is 3 m. This volume allows the air to have a certain distance before reaching the enclosure; being only 0.5 m in width, the mesh does not have an inordinate number of elements to calculate.

The joints between the cladding panels were established at 2 mm, except for the contour, which was 10 mm, and those of each floor, which were 15 mm, in line with the most typical case. Each of the five models corresponds to a different thickness of the air chamber: 1, 3, 5, 10 and 25 cm. The 1 and 25 cm air chambers are outside the scope of the standard, but were also simulated in order to compare the results. Each of the five models was simulated with mild wind ($\times 1$: 4 m/s) and moderate wind ($\times 3$: 12 m/s). The values of wind speed are those seen in Valencia [30], where the normal values between 1971 and 2000 are around 4 m/s, with some peaks above 8 m/s. In this sense, the Spanish standard CTE-SE-AE [31] defines a basic value of wind speed that corresponds to the characteristic value of the average wind speed over a period of 10 min. The characteristic value of the wind speed is the value whose annual probability of being exceeded is 0.02 (return period of 50 years). For a return period of 1 year, the characteristic value set at 26 m/s can be reduced by 0.41, resulting in around 11 m/s.

In this way, we intend to observe the influence of wind on the thermal conditions of the camera and see how air penetration exerts a greater or lesser extent of influence. Winds of greater magnitude, strong or very strong, were not simulated, with the understanding that in such conditions, the problem of stone cladding is its stability. In this research, a winter scenario was also considered, with a temperature difference between the inside and the outside of 20 °C, maintaining theoretical conditions of 20 °C for the interior and 0 °C for the exterior. The ideal temperature for heating in closed spaces is between 19 and 21 °C [32]. Regarding the outside temperature of 0 °C, this is a usual peak in winter in Valencia [33], although the average minimum temperature remains around 5 °C. The relative humidity of the exterior was set high, at 90%, representing a very wet winter day [34]. The relative humidity of the interior was set at 60% since the most accepted range of relative humidity for thermal comfort is from 30 to 70% [35].

Finally, it was assumed that the wind falls directly on the façade, in a leeward scenario. Considering everything that has been described, a study of ten cases was carried out (Table 1).

Table 1. Parameters established for the cases studied.

CASE	Dim. Chamber	Air Veloc.	Joint Dim.	Season	Direction
1	C1: 1 cm	$\times 1$	2 mm	winter	leeward
2	C1: 1 cm	$\times 3$	2 mm	winter	leeward
3	C3: 3 cm	$\times 1$	2 mm	winter	leeward
4	C3: 3 cm	$\times 3$	2 mm	winter	leeward
5	C5: 5 cm	$\times 1$	2 mm	winter	leeward
6	C5: 5 cm	$\times 3$	2 mm	winter	leeward
7	C10: 10 cm	$\times 1$	2 mm	winter	leeward
8	C10: 10 cm	$\times 3$	2 mm	winter	leeward
9	C25: 25 cm	$\times 1$	2 mm	winter	leeward
10	C25: 25 cm	$\times 3$	2 mm	winter	leeward

2.2. Methodology

First, a CAD geometry has been created for each of the five different 3D models. As can be seen in Figure 1a, the model includes a significant volume of air to establish the conditions of the exterior air contour, and thus to be able to appreciate how it moves as it approaches the façade of the building.

The workflow is clearly established from the CFD program. The materials must be assigned for each of the volumes. For the particular case of air, “moist air” was selected to perform the hygrothermal simulation. The thermal insulation material used was polystyrene and, for simplicity, the rest of the elements of stony type were assigned the same stone material. The physical properties of the materials used are shown in Table 2.

Then, the boundary conditions must be assigned. Figure 1a shows the inlet and the outlet for the wind. The rest of the faces of the volume of air have been configured as slip/symmetry to establish the continuity of the model, except for the lower part, which is the floor.

Table 2. Physical properties of the materials used.

Property	Moist Air	Stone	Polystyrene
Density (Kg/m ³)	incompressible	2306	55
Viscosity (Pa·s)	0.001817	-	-
Conductivity (W/m K)	0.02563	1.1	0.027
Specific heat (J/g K)	1.004	0.837	1.21
Emissivity	1	0.92	0.5

Given that this is a very simple geometric model, automatic mesh sizing was enabled so that the program distributes the nodes and finite elements geometry automatically according to the needs of the model. In this case, a smaller mesh was generated around the 2-mm-thick cladding and joints, with a larger mesh in the external air volume (Figure 2). The model consists of approximately 14 K total nodes (13 K fluid nodes, 1 K solid nodes). The minimum mesh is 70 × 2 mm² and the maximum mesh 800 × 800 mm².

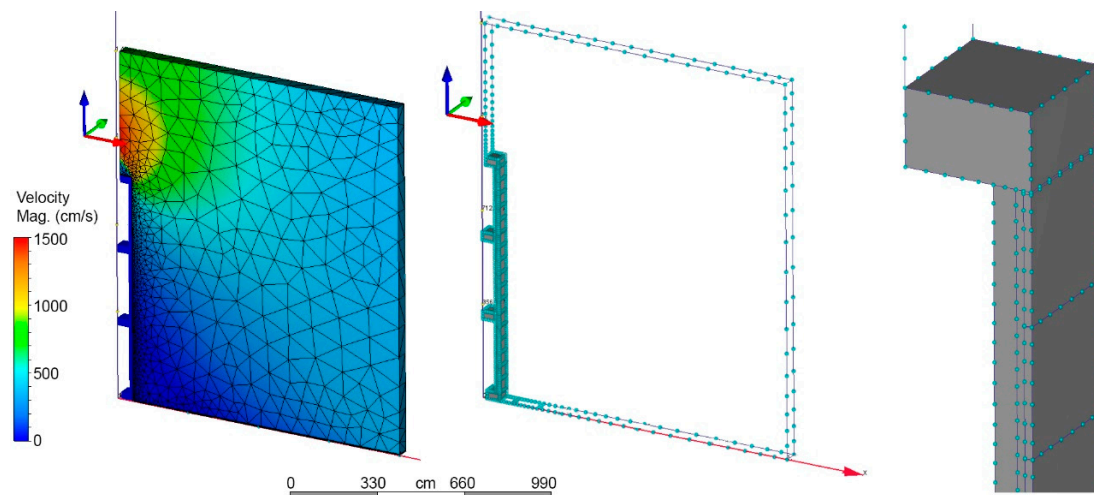


Figure 2. Enabled automatic mesh sizing for the model.

Similarly, to analyse the case of natural convection in the air chamber, the film coefficients in Table 3 were used.

Table 3. Film coefficients used in the calculations.

Flux (W/(m ² ·K))					
Horizontal		Vertical			
		Upward		Downward	
OUT	IN	OUT	IN	OUT	IN
4	35	4	35	4	35

The steady state is of great interest in this case, but not as much the transient state due to the constant temperature gradient that is sought in order to obtain the results. The following physical parameters were considered for the calculation: incompressible flow, hydrostatic pressure, heat transfer, auto forced convection and gravity.

The Navier-Stokes mathematical background provides the equations for fluid flow and heat transfer used by the CFD software [36]. The continuity equation can be written as in Equation (1):

$$\frac{\partial \rho}{\partial t} + \frac{\partial \rho u}{\partial x} + \frac{\partial \rho v}{\partial y} + \frac{\partial \rho w}{\partial z} = 0 \tag{1}$$

The energy equation can be written in terms of static temperature for incompressible and subsonic compressible flow (Equation (2)):

$$\rho C_p \frac{\partial T}{\partial t} + \rho C_p u \frac{\partial T}{\partial x} + \rho C_p v \frac{\partial T}{\partial y} + \rho C_p w \frac{\partial T}{\partial z} = \frac{\partial}{\partial x} \left[k \frac{\partial T}{\partial x} \right] + \frac{\partial}{\partial y} \left[k \frac{\partial T}{\partial y} \right] + \frac{\partial}{\partial z} \left[k \frac{\partial T}{\partial z} \right] + q_v \quad (2)$$

In these equations, C_p is the constant pressure-specific heat; k is the thermal conductivity; q_v is volumetric heat source; T is temperature; t is time; u , v , w , are velocity components in the x -direction, y -direction, and z -direction, and ρ is density.

The energy equation for moist gas flows is written in terms of temperature with a variable specific heat (Equation (3)):

$$\rho \frac{\partial C_p T}{\partial t} + \rho u \frac{\partial C_p T}{\partial x} + \rho v \frac{\partial C_p T}{\partial y} + \rho w \frac{\partial C_p T}{\partial z} = \frac{\partial}{\partial x} \left[k \frac{\partial T}{\partial x} \right] + \frac{\partial}{\partial y} \left[k \frac{\partial T}{\partial y} \right] + \frac{\partial}{\partial z} \left[k \frac{\partial T}{\partial z} \right] + q_v \quad (3)$$

To track the moisture in the fluid, an additional equation is solved for a scalar quantity that represents the mass fraction of the moisture (Equation (4)):

$$\rho \frac{\partial f}{\partial t} + \rho u \frac{\partial f}{\partial x} + \rho v \frac{\partial f}{\partial y} + \rho w \frac{\partial f}{\partial z} = \frac{\partial}{\partial x} \left[D \frac{\partial T}{\partial x} \right] + \frac{\partial}{\partial y} \left[D \frac{\partial T}{\partial y} \right] + \frac{\partial}{\partial z} \left[D \frac{\partial T}{\partial z} \right] + q_v \quad (4)$$

The properties of the moist fluid are calculated assuming a homogenous mixture. With the quality and the mass fraction of the moisture, the mass or mixture fraction of the condensed water can be calculated. This mixture fraction is the output for moist gas calculations along with the relative humidity at every node in the solution domain.

For all the simulations calculated, no fewer than 600 iterations were executed; enough, in this case, for the solution to converge.

Finally, the results were obtained and analysed by comparing the ten cases studied in this research work.

2.3. Validation

To validate the finite elements model, a real building with a ventilated enclosure of stone panels was taken. Thermograms were taken from different points of view and at different times. During the test campaign, an IR camera and temperature and relative humidity sensors were used. All devices were properly calibrated before the measurements according to the operation manual. The reflection calibration, ambient and background compensation of the IR camera were implemented before each measurement.

The emissivity values of the most common construction materials are over 90%, and in our study, we took 0.95 as the default value, and so we believe that the results obtained from the thermographic measurements are reliable [37], and emissivity is practically constant for non-metallic materials [38].

In this study, a FLIR B335 camera was used. It produces thermographic images at a resolution of 320×240 pixels, with a temperature range of -20 to $+120$ °C and an accuracy of less than 50 mK NETD. The thermographic images were subsequently processed with FLIR QuickReport software, which can vary the colour palette, temperature range, distance, as well as calculate the maximum, minimum, and average temperatures in the study areas. The temperature of each pixel in the image can be exported in .csv format.

In other studies [39], façade results obtained by Autodesk Simulation CFD were compared with great precision using additional programs in order to validate ventilated enclosures. Modelling of some thermal phenomena, such as in heat transfer studies of walls, were accomplished with WUFI software. The permeability function of Autodesk Simulation CFD was benchmarked with the theoretical flow rates. A good agreement was achieved utilizing Darcy's equation.

3. Results

3.1. CFD numerical simulation

The results of the simulations show how the air moves towards the building, generating a small turbulence in the lower part of the enclosure (Figure 3a) due to the impossibility of going out in the angle created between the façade and the ground. In Figure 3b, the displacement of some air particles is observed, shown in red.

The simulations make it possible to observe the air particles in movement on the basis of infographics or videos. Figure 4 shows snapshots of this sequence, in which the air is introduced into the chamber through the lower part, increases its temperature, and rises until it leaves the upper part.

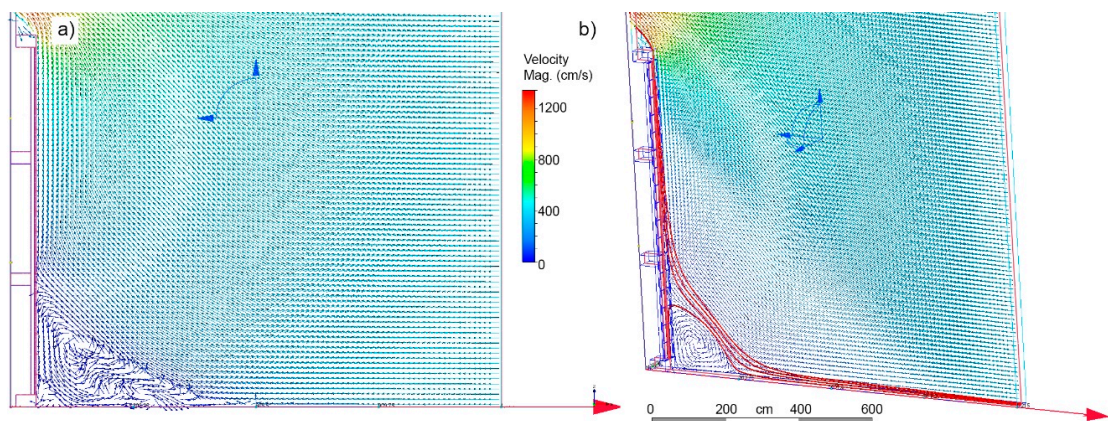


Figure 3. Speed and direction of the air in its encounter with the building: (a) Model elevation and (b) perspective.

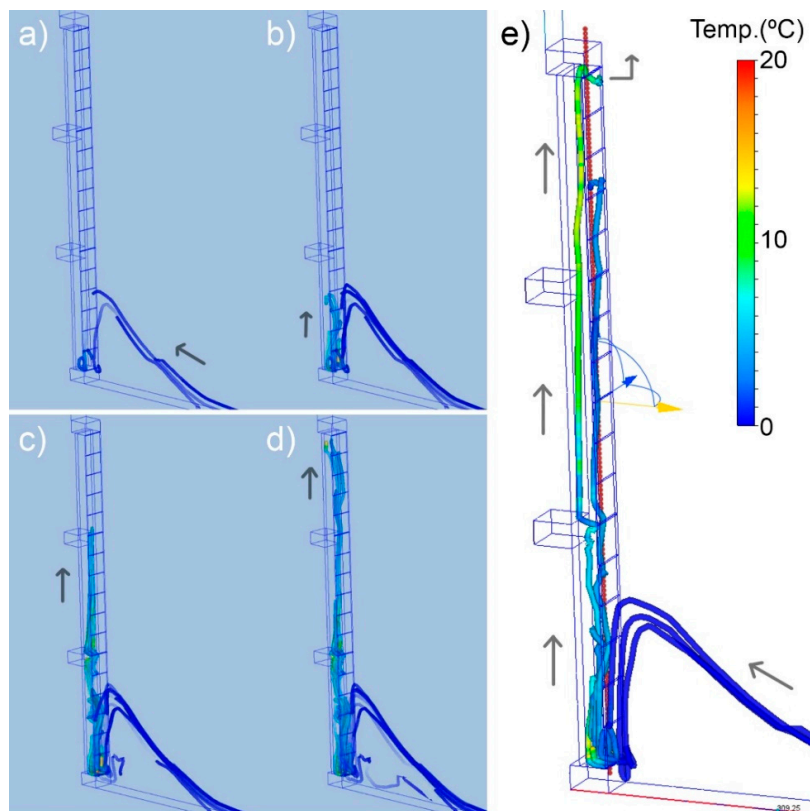


Figure 4. Displacement and temperature of the air particles inside the chamber. From (a–e) steps of the air flow.

Figure 5 shows the temperatures and relative humidity, both with low ($\times 1$) and moderate ($\times 3$) air velocities, for all the air chamber thicknesses studied: 1, 3, 5, 10 and 25 cm. In particular, the cutting plane is located on the outside of the air chamber, that is, on the inside of the stone cladding.

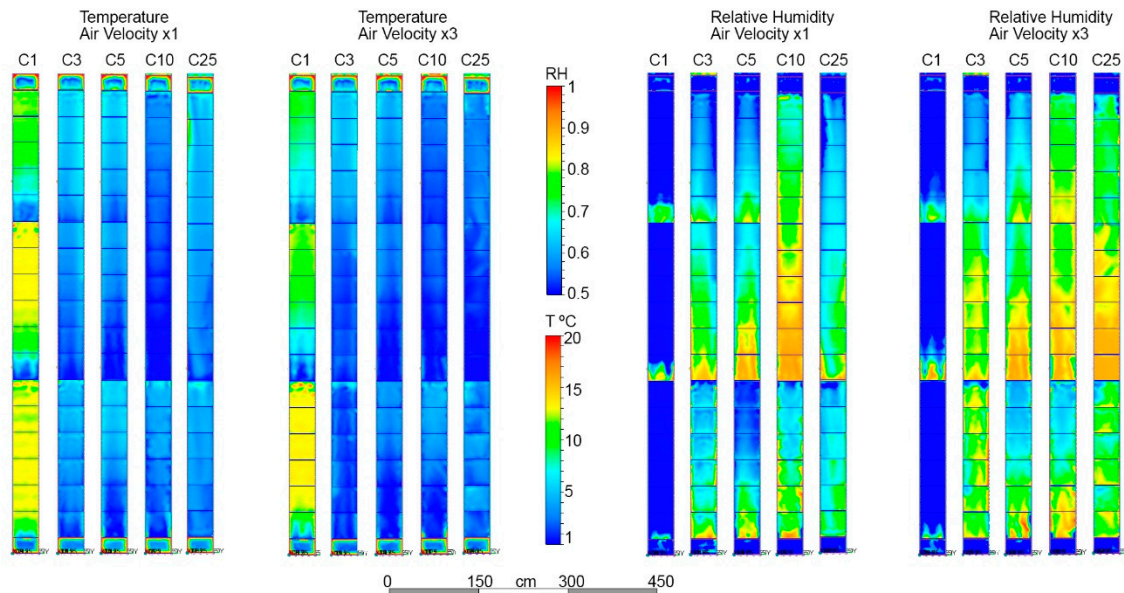


Figure 5. Temperature and humidity for each of the ten cases studied.

Determining temperature and humidity makes it possible to locate the areas that may be susceptible to condensation (low temperatures and high humidity). This condensation is liable to deteriorate the stone material. A better knowledge of the areas in which this condensation may be produced will greatly improve the durability of the material and, therefore, the façade.

This figure makes it possible to establish a qualitative analysis of the hygrothermal behaviour of the air chamber in a stone cladding enclosure with different thicknesses of air chamber and different speeds of external air.

When the thickness of the air chamber is 1 cm, the inside temperature of the building is affected a lot, and the air temperature of the chamber is very high. Infiltrations of cold air from outside are clearly visible. When the air velocity is moderate ($\times 3$), a clear decrease of the temperature inside the chamber is also shown. The relative humidity is high when the air enters the chamber, but it is drastically reduced inside the chamber. If the thickness of the chamber varies from 3 to 10 cm, the temperature decreases with greater thickness of the chamber, and the relative humidity that penetrates the chamber increases with the thickness of the chamber. For chamber thicknesses of 25 cm, being a large dimension, it can be observed that strong convection movements occur, mixing the air at different temperatures before leaving the chamber.

Temperatures are higher and relative humidity is lower on the ground floor than in the upper two (Figure 5). This effect can be explained because the air does not access the air chamber with such ease through the lower part of the enclosure. As can be seen in Figure 3, turbulence occurs in this area.

The following figures make it possible to analyse the data obtained by the simulations.

Figure 6 shows the temperature of a horizontal plane of the air chamber, depending on its thickness and for each of the three floors of the building. The higher temperatures are logically registered together with the thermal insulation (15 °C approx.). Inside the air chamber, the decrease in temperature is more pronounced close to the thermal insulation, and it is less pronounced away from it.

Figure 7 shows the evolution of the temperature inside the air chamber according to its thickness for the ground floor of the building, and considering low air speed ($\times 1$) and moderate speed ($\times 3$). In this way, it is sought to see what the influence is of air velocity on the interior temperature of the air chamber.

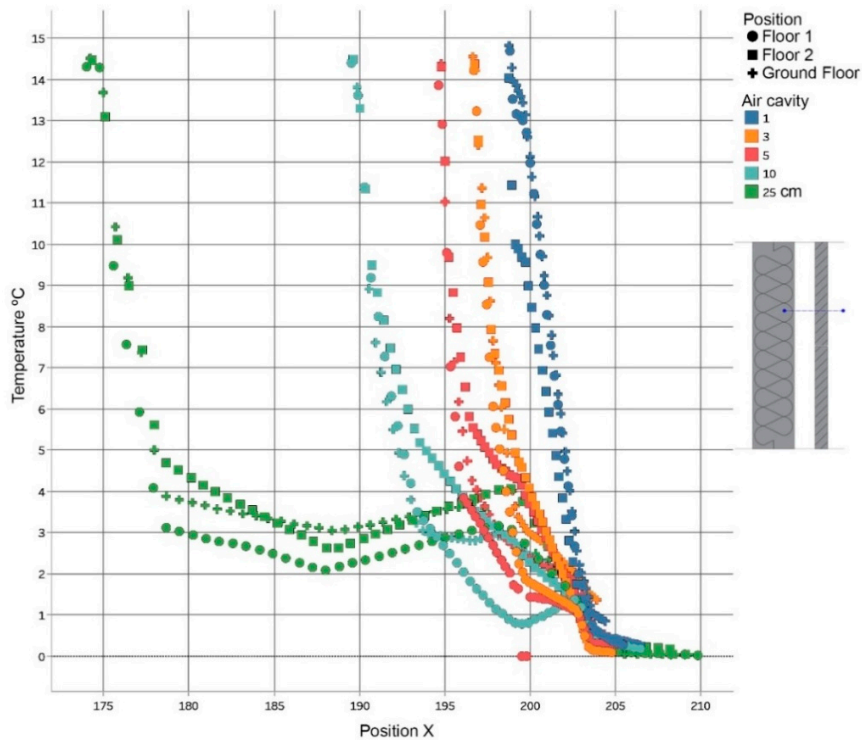


Figure 6. Temperatures in the air chamber, according to the floor and the size of the chamber.

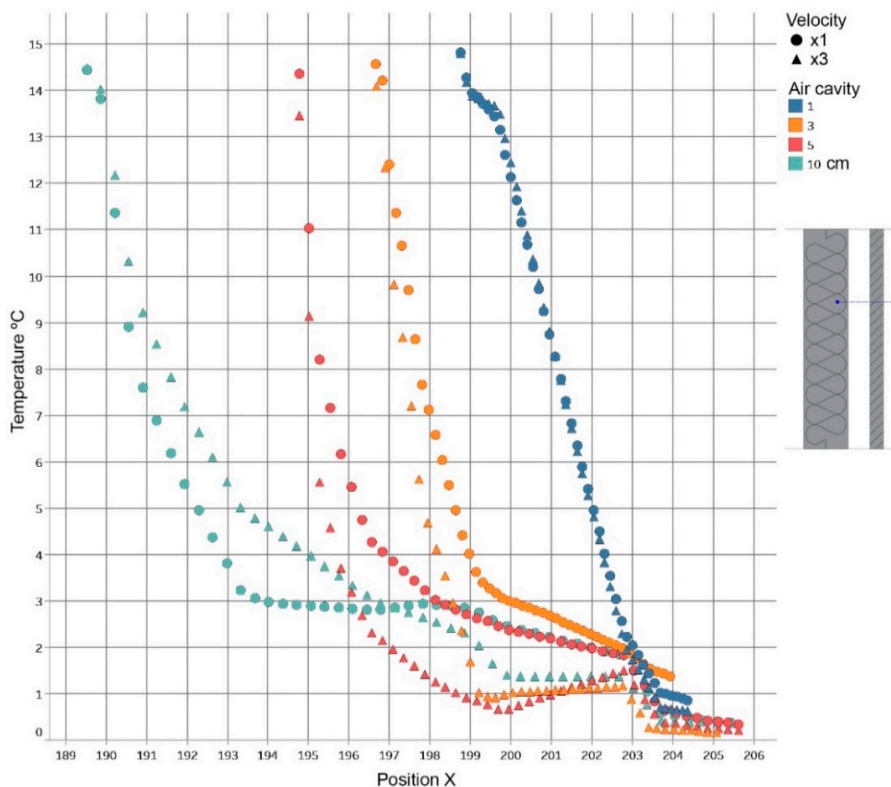


Figure 7. Temperatures in the air chamber, according to wind speed and chamber dimension.

In cases where the air chamber has a thickness of 1 cm, there is no appreciable difference, since the curves on the graph are superimposed. When the camera is 3 or 5 cm, a greater speed of the external air implies a reduction of the interior temperature of the camera when entering a greater volume of cold air. However, for a camera 10 cm thick, this phenomenon does not occur on the ground floor.

The external air velocity ($\times 1$) and the thickness of the air chamber (3 cm) were kept constant in Figure 8. The data was taken in the outermost part of the air chamber (inner face of the stone cladding). This figure compares the relative temperature and humidity values in the three floors of the building. When the temperature is lower and the relative humidity is higher, condensation can occur—liquid water that can affect the material, and which persists over time. In the case studied, the area to be analysed more closely is on the right side of the graph, coinciding with the horizontal joint of 15 mm between the ground floor and the first floor.

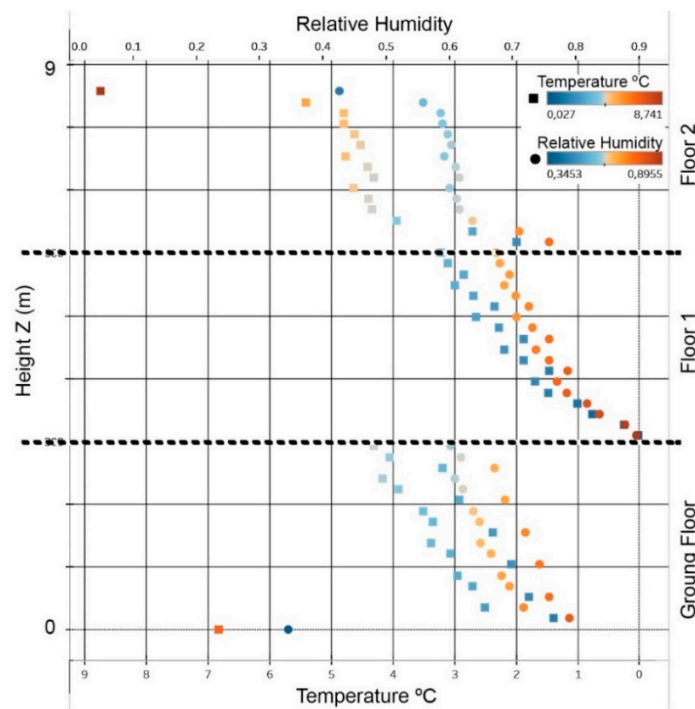


Figure 8. Comparison between relative humidity and temperature to locate possible condensation.

Table 4 shows the variation in temperature and relative humidity for different thicknesses of the air chamber and the different floors of the building, comparing the speed of the soft ($\times 1$) and moderate ($\times 3$) air. The reduction in temperature is more pronounced on the ground floor, with air chamber thicknesses of 3 and 5 cm, up to 27% and 29%, respectively (Table 4a). Regarding relative humidity, the greatest increase occurs in floor 1, with a 1 cm air chamber, up to 29%. Also noteworthy is the 17% increase in the ground floor for the 3 cm air chamber (Table 4b).

Table 4. Temperature and Relative Humidity with variation of air velocity. Darker colour indicates the higher values.

(a)	Temperature	Air Velocity $\times 1$ – $\times 3$				
		C1	C3	C5	C10	C25
	Floor 2	–20%	–12%	–17%	–14%	–13%
	Floor 1	–26%	–26%	–18%	–18%	–1%
	Ground Floor	–2%	–27%	–29%	–8%	–8%
(b)	RH	Air Velocity $\times 1$ – $\times 3$				
		C1	C3	C5	C10	C25
	Floor 2	18%	6%	8%	13%	7%
	Floor 1	29%	10%	6%	8%	3%
	Ground Floor	5%	17%	7%	3%	9%

Table 5 shows the variation of temperature and relative humidity by comparing different thicknesses of the air chamber for smooth (×1) and moderate (×3) air velocity. With a soft air velocity (×1), the temperature is drastically reduced if we compare the thickness of the air chamber of 3 cm with that of 1 cm, with up to a 47% reduction in plant 1 (Table 5a). When the air velocity was moderate (×3) this reduction in temperature increased to 60% with the same air chamber thicknesses (Table 5c).

Regarding relative humidity, this increases to 96% if we compare the 3 cm chamber with the 1 cm chamber in plant 1 with the soft air velocity (×1) (Table 5b). For moderate air velocity (×3), the increase is not so sharp, but importantly, there was an up to 74% increase in relative humidity in the ground floor when comparing the 3 cm air chamber and the 1 cm air chamber (Table 5d).

Table 5. Temperature and Relative Humidity with variation of the thickness of the air chamber. Darker colour indicates the higher values.

(a) Temperature	Air Velocity ×1				(c) Temperature	Air Velocity ×3			
	C3-C1	C5-C3	C10-C5	C25-C10		C3-C1	C5-C3	C10-C5	C25-C10
Floor 2	-31%	-7%	-11%	4%	Floor 2	-24%	-12%	-7%	4%
Floor 1	-47%	-18%	0%	7%	Floor 1	-47%	-8%	-1%	29%
Ground Floor	-46%	-22%	4%	11%	Ground Floor	-60%	-24%	35%	11%

(b) RH	Air Velocity ×1				(d) RH	Air Velocity ×3			
	C3-C1	C5-C3	C10-C5	C25-C10		C3-C1	C5-C3	C10-C5	C25-C10
Floor 2	36%	3%	4%	5%	Floor 2	23%	5%	9%	-1%
Floor 1	96%	-10%	-1%	21%	Floor 1	67%	-13%	0%	16%
Ground Floor	57%	4%	7%	5%	Ground Floor	74%	-5%	2%	11%

Figure 9 compares the temperatures of the air chamber as a function of height, in the interior part (next to the thermal insulation), in the central part of the chamber, and in the exterior part (interior area of the stone cladding). The analysis covers the chamber thicknesses analysed: 1, 3, 5 10 and 25 cm. In all cases, the 1-cm-thick air chamber keeps the temperature very high.

In the inner part of the air chamber, the highest temperatures are reached with the 1, 3 and 25 cm chambers, with the lowest temperatures corresponding to the 5 and 10 cm chambers. In the central part of the chamber, the temperature is clearly reduced, as we increase the thickness of the air chamber. On the outside of the chamber, the temperature reached is very similar regardless of the thickness of the chamber, except for 1 cm, where the temperature remains high.

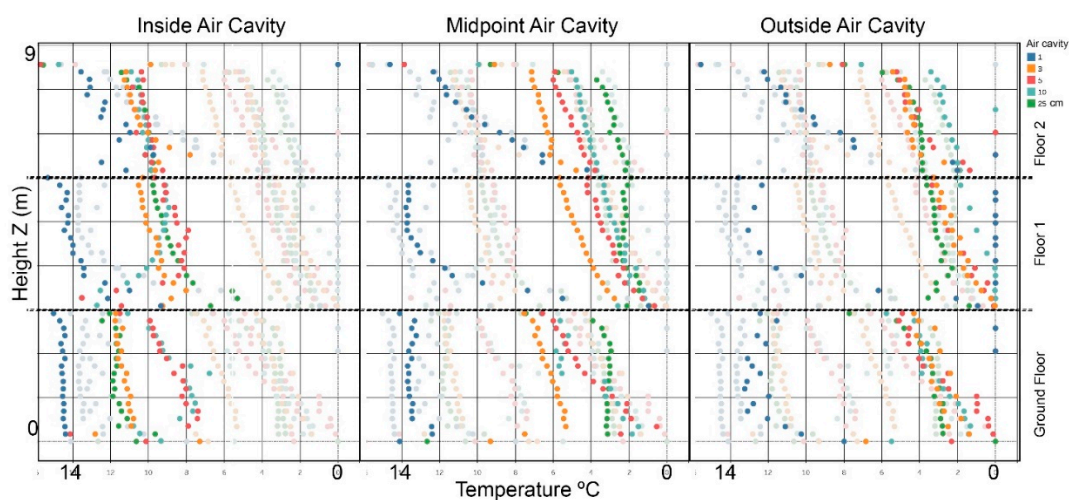


Figure 9. Temperatures reached inside the air chamber depending on its thickness.

3.2. Application of IRT

This research seeks a better knowledge of thermal and moisture behaviour in ventilated enclosures. In addition, it tries to locate those areas susceptible to condensation. IRT facilitates the knowledge of the exterior temperature of each one of the points of the façade. Thus, this real value is used to validate the CFD models.

The thermographic picture makes it possible to obtain the temperature distribution of the enclosure. Figure 10 shows, as an example, a real building with stone cladding. When the results obtained in the simulation vary considerably in a particular area with respect to the thermography, a possible pathology is identified. The climatic conditions of reality differ slightly from those used in the simulations of the previous sections. When thermograms were registered, the outside temperature was 8 °C and the relative humidity was 65%. For this reason, in order to compare, the boundary conditions of reality have been established in a new simulation (Figure 10a).

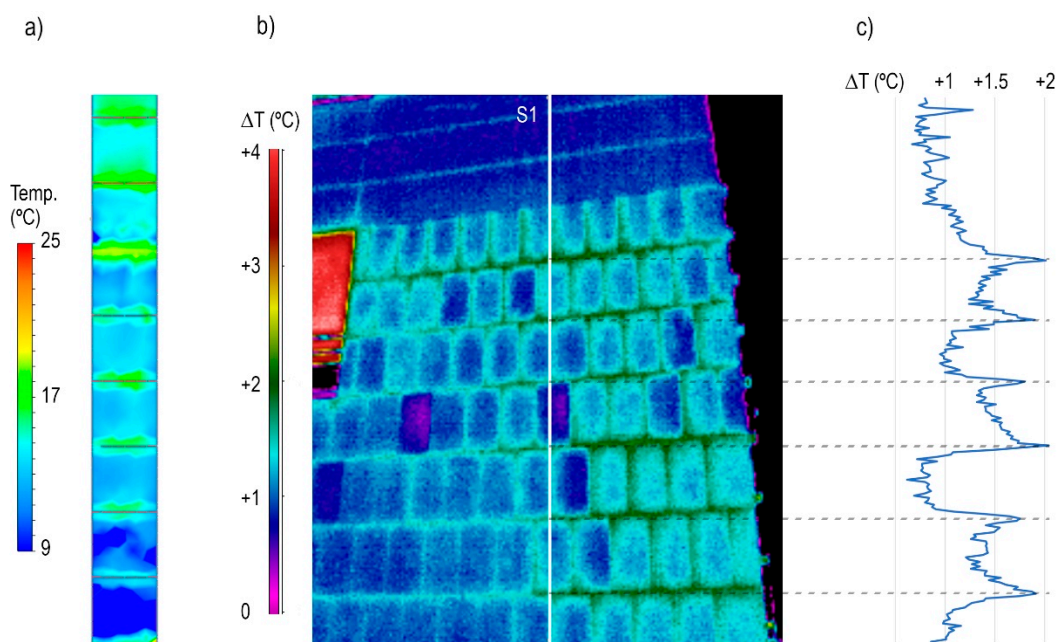


Figure 10. (a) Simulation of enclosure, (b) IRT of a real building, and (c) relative temperatures reached according to the vertical section S1.

Infrared thermography makes it possible to compare real temperature data with simulations to provide more information to the thermodynamic study of the façades of buildings. In Figure 10b, the vertical section S1 can be seen on the thermal picture, whose temperatures are represented in the graph of Figure 10c. This graph shows the variations in temperature, in relative value with respect to the lower temperature of the stone panels. Some peaks in the temperature are observed coinciding with the joints of the stone panels. Figure 10a corresponds to a simulation performed with the boundary conditions of a real building. When examining Figure 10a,b, it is observed that the simulation performed coincides with reality.

4. Conclusions

The results of this work allow a step forward in the knowledge of applying IRT to understand the hygrothermal response in buildings enveloped by stone.

This work underscores the great simulation capacity of finite element models, as well as the possibilities they offers for the exhaustive analysis of stone cladding enclosures. The research focuses on the analysis of the temperature and relative humidity of this type of enclosure, which affects the

possibility of generating condensation and, therefore, the durability of the material. This research work focuses on the development of CFD simulations in buildings located in Valencia (Spain).

Ten models were used to simulate temperature and relative humidity conditions using finite elements and CFD, considering different thicknesses of air chamber and different air speeds. To achieve this, a qualitative and quantitative analysis of the studied models was carried out.

At a qualitative level, the graphical results of temperatures and relative humidity can be compared with different thicknesses of air chamber and air velocity ($\times 1$ and $\times 3$) following real values of Valencia and Spanish standards. In the horizontal section, temperatures drop sharply as soon as we move away slightly from the thermal insulation of the enclosure. With air chambers that are 3 or 5 cm thick, greater speed of the outside air implies a reduction of the interior temperature of the chamber when a greater volume of cold air enters.

A quantitative analysis of the data shows that when comparing the soft ($\times 1$) and moderate ($\times 3$) air velocity the temperature reduction reached 27% with the 3 cm air chamber, and 29% for 5 cm. The relative humidity increased by up to 29% with a 1 cm air chamber and by up to 17% with a 3 cm chamber.

With regard to different air chamber thicknesses, with smooth air velocity ($\times 1$), the temperature is drastically reduced when comparing the thickness of the air chamber of 3 cm with respect to that of 1 cm, with up to a 47% reduction. When the air speed is moderate ($\times 3$), this reduction in temperature increases by up to 60% when comparing the same air chamber thicknesses. Regarding the relative humidity, this increases by up to 96% when we compare the 3 cm chamber with the 1 cm chamber and with the soft air speed ($\times 1$). For moderate air velocity ($\times 3$), the increase is not so sharp, but important, with up to a 74% increase in the relative humidity when comparing the air chambers of 3 cm and 1 cm.

The real value of the outside temperature of the enclosure can be obtained by means of infrared thermography, which facilitates the determination of the exterior temperature of each of the points of the façade in a non-invasive way. Thus, this real value is used to validate the CFD models. When the results obtained in the simulation vary considerably in a given area with respect to thermography, a possible pathology is identified. This work provides better knowledge on the durability of material and façades.

Author Contributions: Investigation, C.L.; Methodology, Á.M.; Validation, E.G.; Writing—original draft, C.L.; Writing—review & editing, J.V.

Conflicts of Interest: The authors declare no conflict of interest.

References

1. Garden, G.K. Rain penetration and its control. National Research Council of Canada. *Can. Build. Dig.* **1963**, *40*, 4.
2. De Vahl Davis, G. Natural convection of air in a square cavity. *Int. J. Numer. Methods Fluids* **1983**, *3*, 249–264. [[CrossRef](#)]
3. Kaminski, D.A.; Prakash, C. Conjugate natural convection problem in the enclosure with one thick vertical wall. *Int. J. Heat Mass Transf.* **1986**, *12*, 1979–1988. [[CrossRef](#)]
4. Du, Z.G.; Bilgen, E. Coupling of wall conductivity with natural convection during a rectangular enclosure. *Int. J. Heat Mass Transf.* **1992**, *35*, 1962–1975. [[CrossRef](#)]
5. Hakyemez, E.; Mobedi, M.; Oztotop, H.F. Effects of wall-located heat barrier on conjugate conduction and natural convection heat transfer and fluid flow in enclosures. *Numer. Heat Transf.* **2008**, *54*, 197–220. [[CrossRef](#)]
6. Kuehn, T.H.; Maldonado, E.A.B. Two-dimensional transient heat transfer through composite wood frame walls—Field measurements and modeling. *Energy Build.* **1984**, *6*, 55–66. [[CrossRef](#)]
7. Al-Sanea, S.A.; Zedan, M.F. Effect of thermal bridges on transmission loads and thermal resistance of building walls under dynamic conditions. *Appl. Energy* **2012**, *98*, 584–593. [[CrossRef](#)]
8. Vercher, J.; Lerma, C.; Vidal, M.; Gil, E. Analysis of energy efficiency in construction solutions at the façade-slab connection. *Adv. Mater. Res.* **2013**, *787*, 731–735. [[CrossRef](#)]

9. Mas, Á.; Gutiérrez, J.; Gil, E.; Gil, A.; Galvañ, V. Design and construction recommendations to improve impermeability in rainscreen walls built with natural Stone coverings. *Constr. Build. Mater.* **2011**, *25*, 1753–1761. [CrossRef]
10. Kumar Patidar, A.; Kannan, M.R. Simulation of conjugate heat transfer and natural convection in the unfilled cavity-walls of building using ADINA-CFD. *Int. J. Civ. Struct. Environ. Infrastruct. Eng. Res. Dev. (IJCSEIERD)* **2013**, *3*, 165–174.
11. Kersten, B.; Schijndel, J. Modeling the heat exchange in cavities of building constructions using comsol multiphysics®. In Proceedings of the 2013 COMSOL Conference in Rotterdam, Rotterdam, The Netherlands, 23–25 October 2013.
12. Rousseau, M.Z. Facts and fictions of rain-screen walls. *Constr. Can.* **1990**, *32*, 42–44.
13. Salonvaara, M.H.; Karagiozis, A.N.; Pazera, M.; Miller, W. Air cavities behind claddings—What have we learned? In Proceedings of the Thermal Performance of the Exterior Envelopes of Whole Buildings Tenth International Conference, Clearwater Beach, FL, USA, 2–7 December 2007.
14. Finch, G.; Straube, J. Ventilated wall claddings: Review, field performance and hygrothermal modeling. In Proceedings of the Thermal Performance of the Exterior Envelopes of Whole Buildings Tenth International Conference, Clearwater Beach, FL, USA, 2–7 December 2007; ASHRAE Publications: Atlanta, GA, USA.
15. Falk, J.; Sandin, K. Ventilated rainscreen cladding: Measurements of cavity air velocities, estimation of air change rates and evaluation of driving forces. *Build. Environ.* **2013**, *59*, 164–176. [CrossRef]
16. Cumo, F.; Astiaso Garcia, D.; Stefanini, V.; Tiberi, M. Technologies and strategies to design sustainable tourist accommodations in areas of high environmental value not connected to the electricity grid. *Int. J. Sustain. Dev. Plan.* **2015**, *10*, 20–28. [CrossRef]
17. Pagliaro, F.; Cellucci, L.; Burattini, C.; Bisegna, F.; Gugliermetti, F.; de Lieto Vollaro, A.; Salata, F.; Golasi, I. A methodological comparison between energy and environmental performance evaluation. *Sustainability* **2015**, *7*, 10324–10342. [CrossRef]
18. Odewole, A.; Edwards, R. The characteristics of the velocity field in a slot-ventilated wall cavity. *ARPN J. Eng. Appl. Sci.* **2011**, *6*, 47–55. Available online: http://www.arpnjournals.com/jeas/research_papers/rp_2011/jeas_1011_570.pdf (accessed on 25 June 2019).
19. Autodesk Simulation CFD Help Desk. 2019. Available online: <https://knowledge.autodesk.com/support/cfd/downloads/caas/downloads/content/cfd-2016-download-and-install-help-documentation.html> (accessed on 15 July 2019).
20. Moropoulou, A.; Avdelidis, N.P.; Karoglou, M.; Delegou, E.T.; Alexakis, E.; Keramidas, V. Multispectral Applications of Infrared Thermography in the Diagnosis and Protection of Built Cultural Heritage. *Appl. Sci.* **2018**, *8*. [CrossRef]
21. Fitzner, B. *Técnicas de Diagnóstico Aplicadas a la Conservación de los Materiales de Construcción en los Edificios Históricos*; Junta de Andalucía: Seville, Spain, 1996.
22. Lerma, C. *Análisis Arquitectónico y Constructivo del Real Colegio de Corpus Christi de Valencia*. Ph.D. Thesis, Universitat Politècnica de València, Valencia, Spain, 2012.
23. De Freitas, S.S.; De Freitas, V.P.; Barreira, E. Detection of façade plaster detachments using infrared thermography—A nondestructive technique. *Constr. Build. Mater.* **2014**, *70*, 80–87. [CrossRef]
24. Danese, M.; Demsar, U.; Masini, N.; Charlton, M. Investigating material decay of historic buildings using visual analytics with multi-temporal infrared thermographic data. *Archaeometry* **2010**, *52*, 482–501. [CrossRef]
25. Campbell, J.B. *Introduction to Remote Sensing*, 2nd ed.; Taylor & Francis: London, UK, 1996.
26. Lerma, C.; Barreira, E.; Almeida, R.M.S.F. A discussion concerning active infrared thermography in the evaluation of buildings air infiltration. *Energy Build.* **2018**, *168*, 56–66. [CrossRef]
27. Meola, C.; Carlomagno, G.M.; Giorleo, L. The use of infrared thermography for materials characterization. *J. Mater. Process. Technol.* **2004**, *155*, 1132–1137. [CrossRef]
28. AENOR. *UNE 22203-2011 Standard. Natural Stone Products. Construction of Slabs for Façade with Natural Stone*; AENOR: Madrid, Spain, 2011.
29. Ministerio de Fomento. *Spanish Standard CTE-DB-HS: Código Técnico de la Edificación, Documento Básico, Salubridad*; Ministerio de Fomento: Madrid, Spain, 2017; Available online: <https://www.codigotecnico.org/images/stories/pdf/salubridad/DBHS.pdf> (accessed on 15 June 2019).

30. IDAE, Spanish Institute for Diversification and Energy Saving. Technical Guide for the External Climatic Conditions of the Project. Available online: https://www.idae.es/uploads/documentos/documentos_12_Guia_tecnica_condiciones_climaticas_exteriores_de_proyecto_e4e5b769.pdf (accessed on 17 July 2019).
31. Ministerio de Fomento. *Spanish Standard CTE-SE-AE: Código Técnico de la Edificación, Documento Básico, Seguridad Estructural, Acciones en la Edificación*; Ministerio de Fomento: Madrid, Spain, 2017; Available online: <https://www.codigotecnico.org/images/stories/pdf/seguridadEstructural/DBSE-AE.pdf> (accessed on 15 June 2019).
32. IDEA. Spanish Institute for Diversification and Energy Saving. Available online: https://www.idae.es/uploads/documentos/documentos_Guia_007_Frecuencias_horarias_repeticion_en_temperatura_Intervalo_24_h_a7945051.pdf (accessed on 17 July 2019).
33. Martínez, F.; Moya, C.; Rodríguez, M.; Requena, R.; Briz, Á.; Moshuk, M.; Morales, T.; Rivas, G.; Morala, J.F.; Badenes, J.; et al. *Statistics Summary of the City of Valencia (Spain)*; Valencia City Council: Valencia, Spain, 2018; Available online: http://www.valencia.es/ayuntamiento/webs/estadistica/Recull/Recull2018_Ingles.pdf (accessed on 17 July 2019).
34. Weather Online. Relative Humidity Values 2015–2019. Available online: <https://www.woespana.es/weather/maps/city?LANG=es&WMO=08284&ART=RLF&CONT=eses&R=0&LEVEL=150®ION=0005&LAND=SP&NOREGION=1&MOD=&TMX=&TMN=&SON=&PRE=&MONAT=&OFFS=&SORT=&MM=01&YY=2019&WEEK=200> (accessed on 15 July 2019).
35. Olgyay, V. *Design with Climate, Bioclimatic Approach to Architectural Regionalism*; Princeton University Press: Princeton, NJ, USA, 2015; ISBN 9780691169736. Available online: <https://press.princeton.edu/titles/10603.html> (accessed on 17 July 2019).
36. Autodesk Simulation CFD Help Desk. 2019. Available online: <https://knowledge.autodesk.com/support/cfd/learn-explore/caas/CloudHelp/cloudhelp/2018/ENU/SimCFD-Learning/files/GUID-83A92AE5-0E9E-4E2D-B61F-64B3696E5F66-htm.html> (accessed on 15 July 2019).
37. Rodríguez Liñán, C. Inspección mediante técnicas no destructivas de un edificio histórico: Oratorio San Felipe Neri (Cádiz). *Inf. Constr.* **2011**, *63*, 13–22. [CrossRef]
38. Cañas, I. Thermal-physical aspects of materials used for the construction or rural buildings in Soria (Spain). *Constr. Build. Mater.* **2005**, *19*, 197–211.
39. Doggett, M.S.; Brunjes, R.F. Simulation of Convective Heat Loss through Mineral Wool in a Rainscreen Façade. Presentation to Minnesota Building Enclosure Council, 24 May 2016. Available online: <https://bec-mn.org/wp-content/uploads/2016/05/convective-heat-loss-through-mineral-wool-in-rainscreen-facades-0526161.pdf> (accessed on 16 July 2019).



© 2019 by the authors. Licensee MDPI, Basel, Switzerland. This article is an open access article distributed under the terms and conditions of the Creative Commons Attribution (CC BY) license (<http://creativecommons.org/licenses/by/4.0/>).